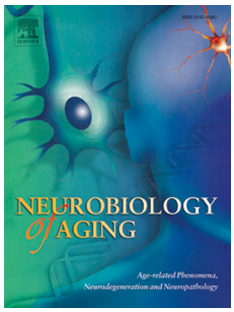

Spatial Gradients Of Healthy Ageing: A Study Of Myelin-Sensitive Maps

Vyacheslav R. Karolis, Martina F. Callaghan, Jane Chieh-En Tseng, Thomas Hope, Nikolaus Weiskopf, Geraint Rees, Marinella Cappelletti

PII: S0197-4580(19)30080-6

DOI: https://doi.org/10.1016/j.neurobiolaging.2019.03.002

Reference: NBA 10529

To appear in: *Neurobiology of Aging*

Received Date: 8 September 2017

Revised Date: 6 February 2019

Accepted Date: 5 March 2019

Please cite this article as: Karolis, V.R., Callaghan, M.F., Chieh-En Tseng, J., Hope, T., Weiskopf, N., Rees, G., Cappelletti, M., Spatial Gradients Of Healthy Ageing: A Study Of Myelin-Sensitive Maps, *Neurobiology of Aging* (2019), doi: https://doi.org/10.1016/j.neurobiolaging.2019.03.002.

SPATIAL GRADIENTS OF HEALTHY AGEING: A STUDY OF MYELIN-SENSITIVE MAPS

Vyacheslav R. Karolis[1,2], Martina F. Callaghan[3], Jane Chieh-En Tseng[2,4], Thomas Hope[3], Nikolaus Weiskopf[3,5], Geraint Rees[6], Marinella Cappelletti[6,7]

[1] FMRIB centre, John Radcliffe Hospital, University of Oxford, UK

[2] Institute of Psychiatry, Psychology, and Neuroscience, King's College London, London, UK.

[3] Wellcome Trust Centre for Nesuroimaging, UCL Institute of Neurology, 12 Queen Square, London, UK.

[4] Department of Radiology, Massachusetts General Hospital, Harvard Medical School, Charlestown, USA

[5] Department of Neurophysics, Max Planck Institute for Human Cognitive and Brain Sciences, Leipzig, Germany.

[6] UCL Institute of Cognitive Neuroscience, 17 Queen Square, London, UK.

[7] Psychology Department, Goldsmiths University of London, UK.

ABSTRACT

Protracted development of a brain network may entail greater susceptibility to ageing decline, supported by evidence of an earlier onset of age-related changes in late-maturing anterior areas, i.e. an anterior-to-posterior gradient of brain ageing. Here we analysed the spatio-temporal features of age-related differences in myelin content across the human brain indexed by magnetisation transfer (MT) concentration in a cross-sectional cohort of healthy adults. We described age-related spatial gradients in MT, which may reflect the reversal of patterns observed in development. We confirmed an anterior-to-posterior gradient of age-related MT decrease, and also showed a lateral-to-ventral gradient inversely mirroring the sequence of connectivity development and myelination. MT concentration in the lateral white matter regions continued to increase up to the age of 45, and decreased moderately following a peak. In contrast, ventral white matter regions reflected life-long stable MT concentration levels, followed by a rapid decrease at a later age. We discussed our findings in relation with existing theories of brain ageing, including the lack of support for the proposal that areas which mature later decline at an accelerated rate.

Keywords:

Ageing, gradient, maturation, myelin, magnetisation transfer

1. INTRODUCTION

Brain development is associated with asynchronous anatomical alterations in macro- and microstructure, with different regions maturing at different times and rates (Deoni et al., 2011; Gogtay et al, 2004; Sowell et al, 2004). In white matter, corticospinal and thalamocortical connectivity, supporting basic sensory and motor functions, is the first to develop, followed by the proliferation of unilateral cortico-cortical connections once the thalamo-cortical connections have grown into the cortical plate (Kostovic and Jovanov-Milošević 2006). Flechsig's Law of Myelogenesis (Flechsig, 1901) proposes that the sequence of myelination is linked to the development of functional systems. In support of this, a ventral-to-lateral gradient of maturation characterises the process of axon myelination (Kinney et al, 1988; Yakovlev and Leours 1967). Cortico-cortical connections are more likely to develop for longer as they play a critical role in supporting high-level adaptive behaviour (Catani et al, 2012; Kinney et al, 1988). A protracted development of language networks (Gogtay et al, 2004; Sowell et al., 2003), with their left hemisphere dominance, may also explain greater postnatal myelin growth in the left compared to the right hemisphere in the posterior brain (Deoni et al., 2011).

How this asynchronous maturation across the brain might subsequently affect the process of ageing remains an open question. One possibility is 'last-in, first-out', i.e., the temporal sequences of maturation and ageing are inversely related (Douaud et al, 2014; Raz, 2000; Reisberg et al, 1999). Whilst the exact mechanisms for this pattern are not known, it has been suggested that protracted development of a brain network, which may continue at least as late as the third decade from birth (Somel et al. 2009; Lebel and Beaulieu 2011), would entail a greater exposure to adverse environmental factors, and subsequently result in a greater susceptibility to ageing decline (Casey et al, 2000). Changes in the regenerative abilities of the brain may also play a role. For example, monkey studies suggest that despite a continued production of myelin

in ageing monkeys, the sheaths of myelin formed later in development are easier to break down (Peters et al, 2001) and therefore less stable.

In line with this 'last-in, first-out' (retrogenesis) principle, grey matter volume in late-maturing prefrontal regions typically starts declining earlier than in posterior regions (Davis et al, 2008; Gogtay et al, 2004; Raz et al, 1997, 1998). An anterior-to-posterior gradient of ageing also emerges in white matter microstructure, with greater fractional anisotropy (FA) (Basser et al, 1994) decreases observed in prefrontal white matter and in the anterior part of the corpus callosum compared to posterior areas (Salat et al, 2005a, 2005b).

The existing evidence does not, however, support the retrogenesis perspective unambigously. For example, phylogenetically old medial temporal regions which mature early, like the hippocampus and entorhinal cortex (Gogtay, 2004; Shaw et al, 2008), nevertheless show accelerated volume shrinkage with age (Fjell et al, 2014; Raz et al, 2005, but see Bigler et al, 1997) and have been implicated in neurodegenerative disorders (Schmitz et al, 2016; West et al, 1994). FA also decreases in the cerebral peduncles and in the posterior limb of the internal capsule containing early-myelinating fibres of the corticospinal tract (Brickman et al, 2012; Salat et al, 2005a, 2005b).

Two views of retrogenesis can be further distinguished. One focuses on the spatial layout of age-related changes and assumes greater differences between young and older adults in the later maturing regions as a result of an earlier onset of ageing (e.g., Head et al., 2004). The other view instead emphasises the dynamic features of ageing by proposing that later maturing brain areas are characterised by an accelerated rate – not by an earlier onset - of decline (Bender, Völkle, & Raz, 2016; Douaud et al, 2014; Sexton et al, 2014).

In white matter ageing research, these inconsistent findings may result from the limited specificity of FA measures (Deoni et al, 2008; Jones et al, 2012), as various factors contributing

to FA may be differentially affected by ageing. For instance, myelin is just one of at least four major contributors to the FA signal (Jones et al, 2012), with the sensitivity of FA to crossing fibres complicating the interpretation of any local increases or decreases (Douaud et., 2011). Therefore, it is not clear whether the 'last-in, first-out' principle is applicable to age-related myelin changes. The issue may be resolved by exploiting a more detailed characterisation of microstructural content, which may in turn also reveal new spatial gradients of ageing beyond the anterior-to-posterior gradient, as predicted from developmental studies (Deoni et al, 2011; Kinney et al, 1988; Kostovic and Jovanov-Milošević 2006; Yakovlev and Leours 1967).

In the present study, we capitalised on the past developmental findings to test specific predictions concerning the spatial and temporal features of age-related differences in white matter. We collected magnetisation transfer saturation maps (MT) (Helms et al, 2008; Weiskopf et al, 2013) in a large cross-sectional sample of adults. MT maps show high correlations with myelin content measured histologically (e.g., Schmierer er al., 2007). Given the cross-sectional character of the data, the present study refers to "age-related differences" to denominate the individual variability that is collinear with a participant's age. We hypothesised that in addition to an anterior-to-posterior spatial gradient of healthy ageing, other gradients, such as a left-to-right and a lateral-to-ventral, may emerge as a reflection of the asynchrony in structural brain development. By analysing the patterns of age-related differences, we also sought to investigate any temporal features of ageing whereby regions that reach a maturation peak late may show an accelerated rate of change of age-related differences following the peak.

2. METHODS

2.1 Participants

Ninety-seven healthy high-functioning participants without neurological or psychiatric disease and with no contraindications to MRI (40 males, 57 females; mean age: 46.4, age range: 20-74) provided written informed consent to take part in the MRI study approved by the local ethics committee. All participants above the age of 34 years old received the Mini Mental State Examination (MMSE, Folstein et al, 1975) and achieved a score of 28 or greater, suggesting that their cognitive faculties were within the normal range. Four ageing participants reported taking medications for either hypertension or high cholesterol. None of the participants reported being diabetics. See Table 1 for a summary of the participants' demographic features.

Table 1. Demographic features of the participants

	Gender	**Mean age (SD)**	**Years of education (SD)**	**MMSE (median & range)**	**Handedness**
Young (*n* = 29)	11M, 18F	26.4 (4.7)	17.6 (2.1)	NA	1 L, 28 R
Middle (*n* =38)	17M, 21F	46.6 (6.7)	17.1 (3.2)	30 (27-30)	3 L, 35 R
Older (*n* = 30)	12M, 18F	65.9 (4.3)	16.0 (2.9)	30 (28-30)	3 L, 28 R
Total/Mean	40M, 57F	46.3 (5.2)	16.9 (2.7)	30 (28-30)	7 L, 91 R

Legend
SD=standard deviation
M= males, F= females
MMSE= Mini-Mental State Examination
NA= not applicable

L=left, R=right

2.2 Data Acquisition

All participants were scanned using the same protocol and hardware. A whole-brain quantitative multi-parameter mapping (MPM) protocol implemented at the Wellcome Trust Centre for Neuroimaging (WTCN) in London was used on a 3T whole body MR system (Siemens Healthcare, Erlangen, Germany) equipped with a standard 32-channel head coil for receive and radiofrequency transmission. Following an established paradigm (Callaghan et al, 2014a; Lutti et al, 2010, 2012; Weiskopf et al, 2013), the MPM protocol consisted of three spoiled multi-echo 3D fast low angle shot (FLASH) acquisitions with 1mm isotropic resolution and two additional calibration sequences to correct for inhomogeneities in the RF transmit field. The FLASH volumes were acquired with predominantly proton density or T_1 weighting, as determined by the repetition time and flip angle combination. MT weighting was achieved through the application of an off-resonance pulse prior to excitation. Quantitative MT saturation was calculated from the acquired images using an in-house MATLAB program. The method has been previously shown to inherently account for inhomogeneities of the receive coil and the transmitted RF field (Helms et al., 2008). The relationship of magnetisation transfer signal to the content of myelin has been previously demonstrated in histological studies of ex-vivo multiple sclerosis patients and animal models (Ou et al., 2009; Schmierer et al., 2007; 2008).

2.3 Image co-registration

The preprocessing pipeline is shown in Figure 1. To improve the separation between brain and non-brain tissues in MT maps, non-brain tissues were masked out using participants' T1-

weighted and proton density (PD*) maps (Callaghan et al, 2014), linearly co-registered with MT maps. Brain extraction implemented in FSL BET was performed on T1-weighted and PD* maps, and the two masks outputted by this process were used to create a common Boolean-AND brain mask. Individual MT maps were multiplied by the mask and were once again submitted to BET using a low value for the fractional intensity threshold *f* for an additional clean-up of the non-brain tissues. The results were visually checked for quality and manually adjusted for incorrectly excluded brain voxels.

A study-specific whole-brain template and diffeomorphic transformations between native and standard spaces were generated using the Greedy symmetric diffeomorphic normalization GreedySyN pipeline distributed with the Advanced Normalization Tools (http://stnava.github.io/ANTs; Avants et al, 2011), a joint top-performing normalisation method among 14 common methods (Klein et al, 2009). Once an initial affine template was created, four iterations of the nonlinear refinement were performed. The template was co-registered linearly with the ICBM152 MNI template.

2.4 Calculation of standardised quantitative maps

The standardised quantitative maps were obtained using the procedure outlined in Draganski et al (2011), which is a modified version of the T-SPOON algorithm proposed in Lee et al. (2009). Following this method, tissue-specific parameter maps are produced while optimally preserving the quantitative parameter values within each tissue class and reducing effects of residual mis-registration and partial volume effects (Draganski et al., 2011; Lee et al., 2009). The following steps were performed. Firstly, grey (GM) and white matter (WM) tissue probability maps (TPM) were obtained from the MT maps in native space using the unified segmentation approach implemented in SPM12. The TPMs were then warped into the standard space and scaled by the

Jacobian determinants of the deformation field. A combined probability weighting and Gaussian smoothing (using a 6mm FWHM isotropic smoothing kernel) was then applied to the WM quantitative maps whereby each participant's quantitative maps in the standard space were, in exact order, multiplied by an unsmoothed modulated TPM, smoothed, and then divided by a smoothed modulated TPM (see Figure 1). The use of modulated weighting prior to the application of the Gaussian filter is the main modification to the T-SPOON algorithm, allowing compensation for the effect of the individual variability in the brain size (Draganski et al., 2011) (the effect of modulation is then undone by dividing with the smoothed modulated images) and hence decreasing the partial volume effects. Finally, group-average masks were generated by thresholding individual probability maps for each tissue class at 0.2 and then averaging them across all participants. Each voxel was subsequently assigned to a tissue class for which an average probability value was maximal. This approach was used to ensure that each voxel was analysed in only one subspace (Callaghan et al, 2014). Intracranial volumes were calculated using procedure outlined in (Keihaninejad et al, 2010).

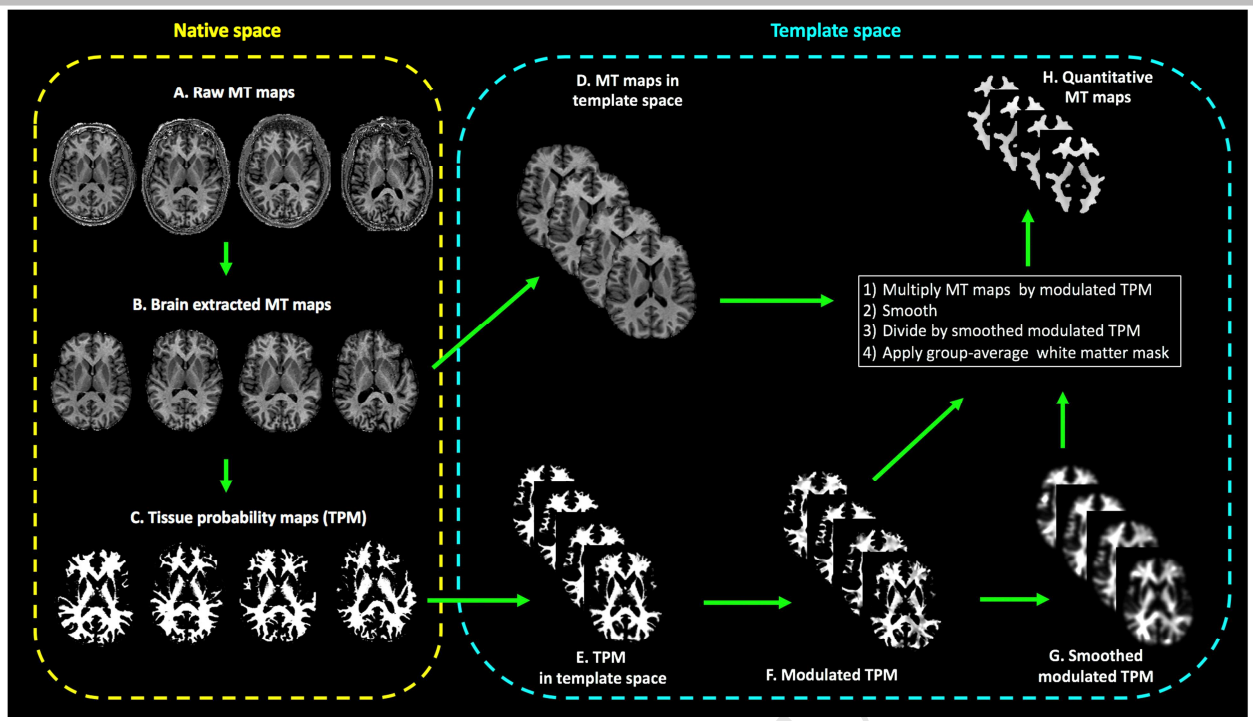

Figure 1. **Preprocessing pipeline**

2.5 Statistical analyses

2.5.1 Outline of statistical approach

Statistical analyses were run in three stages. In the first stage we identified white matter regions showing significant age-related effects and separated linear patterns of age-related differences from non-linear patterns. For this purpose, we used polynomial fits up to a 3rd order as approximations to the trajectories of age-related differences and used model selection procedure to decide which of those best accounted for the data. In the second stage, we compared the inter-regional differences in age-related effects, including inter-hemispheric differences. In the third stage, we investigated spatiotemporal patterns of age-dependent differences, focusing only on the regions which showed non-linear patterns. Specifically, given that ageing is associated with de-myelination, we aimed to estimate the point in the studied age-range at which MT starts

decreasing at a rapid rate. This would serve as a cross-sectional estimate for the time of the onset of age-related decline. For this purpose, we used piecewise linear approximations to non-linear trajectories, provided by a two-component segmented fit. Additional details of the statistical methods are outlined below in Sections 2.5.2 and 2.5.3.

2.5.2 Construction of maps showing age-related effects

Mass-univariate statistical analyses of age-related effects in white matter were carried out using a multiple linear regression model embedded in the general linear model framework of SPM12. To identify and characterize the spatio-temporal features of age-related changes, each voxel was fitted with 3rd order polynomial model using age as a linear, quadratic and cubic predictor. There was a very moderate negative association between years of education and age, r = -.18. Consequently, years of education, together with sex and intracranial volume, was entered as a variable of no interest. Omnibus F-contrast test for all predictors associated with age was run to create a map of significant age-related differences using threshold criterion of $p < .05$ (family-wise corrected). The map was then parcellated further into 'linear' (linear predictor only), '2nd order' polynomial (both a linear and quadratic predictor) and '3rd order' polynomial model maps using likelihood ratio test at each individual voxel.

2.5.3 Inter-regional distributions of age-related effects

The strength of the age-related effects across white matter was quantified using Cohen f^2 for the full model compared to the models containing only the parameters of no interest. Partitioning of white matter into subdivisions was obtained by running Freesurfer white matter parcellation onto the study template. Labelling of the white matter regions was done using John Hopkins

University tractography and ICBM-DTI-81 atlases distributed with FSL. To perform an analysis of the inter-hemispheric differences, MT maps were co-registered with a symmetrical MNI template (available at http://www.bic.mni.mcgill.ca/ServicesAtlases/ICBM152NLin2009). We then obtained the distribution of ageing effects in each voxel in the symmetrical space by means of bootsrapping procedure, whereby we sample 1000 participants sets, randomly with replacement, and obtained the distribution of Cohen's f^2 for each voxel. We then split the effect size maps into the left and right hemisphere maps, flipped X-Y orientation of left hemisphere maps and subtracted them from the corresponding right hemisphere maps. The voxels which showed a larger effect size in one of the hemispheres in 97.5% cases (i.e., approximating $p < .05$, two-tailed) and form clusters of more than 50 voxels were considered as showing significant lateralisation of age-related differences.

2.5.4 Spatiotemporal patterns of age-related differences

In the further analyses of brain regions showing non-linear patterns, we sought to estimate a) the critical points in the trajectory of age-dependent differences at which the gradients of these differences change and b) the gradients of age-related differences preceding and following these points. For a detailed characterisation of these properties, the two-component segmented (aka piecewise) linear fit (Toms and Lesperance. 2003), as implemented in R (Core Team 2015), was applied to the voxels for which a non-linear fit, either 2nd or 3rd order polynomial, outperformed the linear one. Prior to fitting, the data were residualised with respect to intracranial volume, years of education and sex. Three parameters of interest characterise the segmented fit: 1) breakpoint, i.e., a point that separates two linear segments of the fitted function; this parameter was used as an estimate for a critical point in the trajectory; the rate of change of the linear segment 2) before, and 3) after the breakpoint. The latter two characterised how quickly the age-

related differences unfold, prior to and following the critical point on the trajectory, respectively.

A correction of the parameter estimates was performed because the segmented linear fit has no analytical solution and can produce degenerate estimates of parameters if the algorithm minimising the cost function stops at a local minimum. In the first step of this procedure, the parameters of interest were plotted for visual inspection in order to identify any cases of clear degeneracy which may have required refitting if necessary to obtain more appropriate estimates. These cases (1%) showed an estimated breakpoint close to the extrema of the studied age distribution, coupled with abnormal rate of change of the linear segment before or after the breakpoint. This effectively implies a linear trajectory of ageing, which is not supported by the results of the model selection procedure. Next, for a futher improvement of the estimates, the parameters of interest were spatially smoothed (Eklund et al., 2012) by mapping them onto the brain and by applying a Gaussian filter with FWHM of 3 mm. Normalised convolution (Knutsson & Wesitn, 1993) was applied to prevent the effect of the voxels being outside the white matter mask, with weights = 1 if a voxel was within white matter mask and = 0 otherwise. Following this procedure, the parameter estimates represented a weighted average of the parameters in the neighbourhood of the voxel for which the parameter was estimated.

3. RESULTS

3.1 Spatial distribution of linear and non-linear patterns

The spatial extent of significant age-related differences and the best-fitting model maps are shown in Figure 2. These differences, predominantly non-linear, were bilateral in the frontal lobe. More posteriorly, regions showing significant age-related differences were found more frequently in the left than in the right hemisphere. In the left hemisphere, these age-related

differences extended from the parietal lobe into both the occipital and the posterior part of the left temporal lobe. The corpus callosum was relatively unaffected with the exception of the anterior part (genu). Significant age effects did not spread into the anterior or ventral temporal lobes.

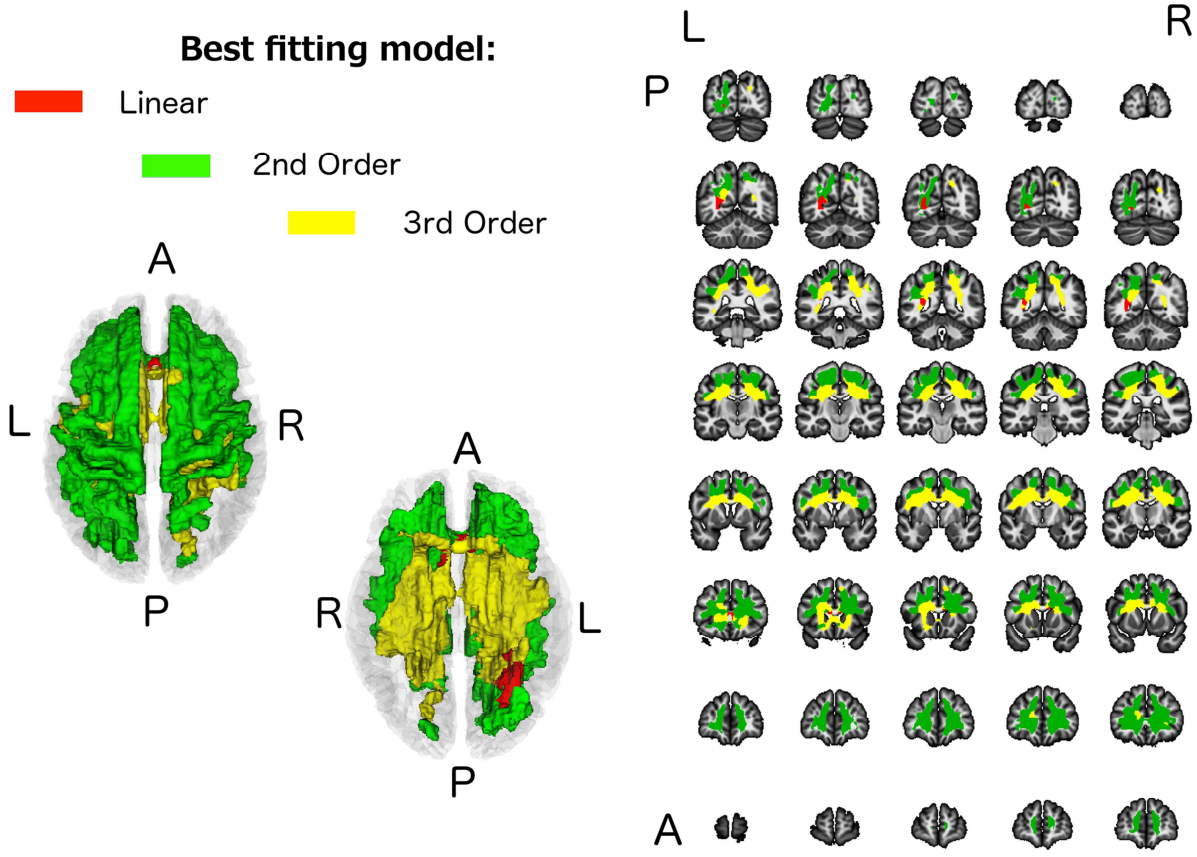

Figure 2. **Spatial distribution of significant linear and non-linear (2nd and 3rd order polynomial fits) age effects in white matter maps.** Left panel: superior and inferior views. Right panel: coronal slices. L – left; R – right; A – anterior; P - posterior

3.2 Effect size

Figure 3A and 3B show the spatial map of age-dependent effect size across white matter and its frequency distributions within white matter parcels, respectively (also see Supplementary Figure 1 for a high resolution version of Figure 3A) The strongest effect can be seen in the frontal lobes (Cohen's f^2 = 0.70, CI= [0.37 1.02]). The anterior-to-posterior spatial gradient can also be

observed in white matter parcels extending in the anterior-to-posterior direction. Thus, the insula, the cingulate (see Supplementary Figure 2) and deep white matter regions were characterised by bimodal distributions, with a stronger effect in the anterior subdivisions of these parcels. The weakest effects of ageing were found in temporal (Cohen's f^2 = 0.30, CI = [0.13 0.56]) and occipital white matter (Cohen's f^2 = 0.27, CI = [0.11 0.48]). Supplementary Figure 3 illustrates that the strength of the age-dependent effects was unaffected by partialling out variances predicted by the PD* and R2* maps which are sensitive to white matter pathology and neurovascular alterations, respectively.

The analysis of age-dependent lateralisation effects identified eight regions where these effects differed significantly between the left and right hemispheres (Figure 3C). In the posterior brain, five white matter regions showed greater age-dependent differences in the left than the right hemisphere: one region anterior to the inferior half of the putamen (intersection of internal and external capsules); two regions in the occipital white matter, one lateral and one medial; white matter under the angular gyrus, likely to be part of arcuate fasciculus; a white matter region situated deeply under the middle frontal gyrus. Age-related effects were stronger in the right hemisphere in three regions: two regions underlying the inferior parts of the pre- and post-central cortices, and one region in the frontal lobe adjacent to the bottom of the cingulate sulcus.

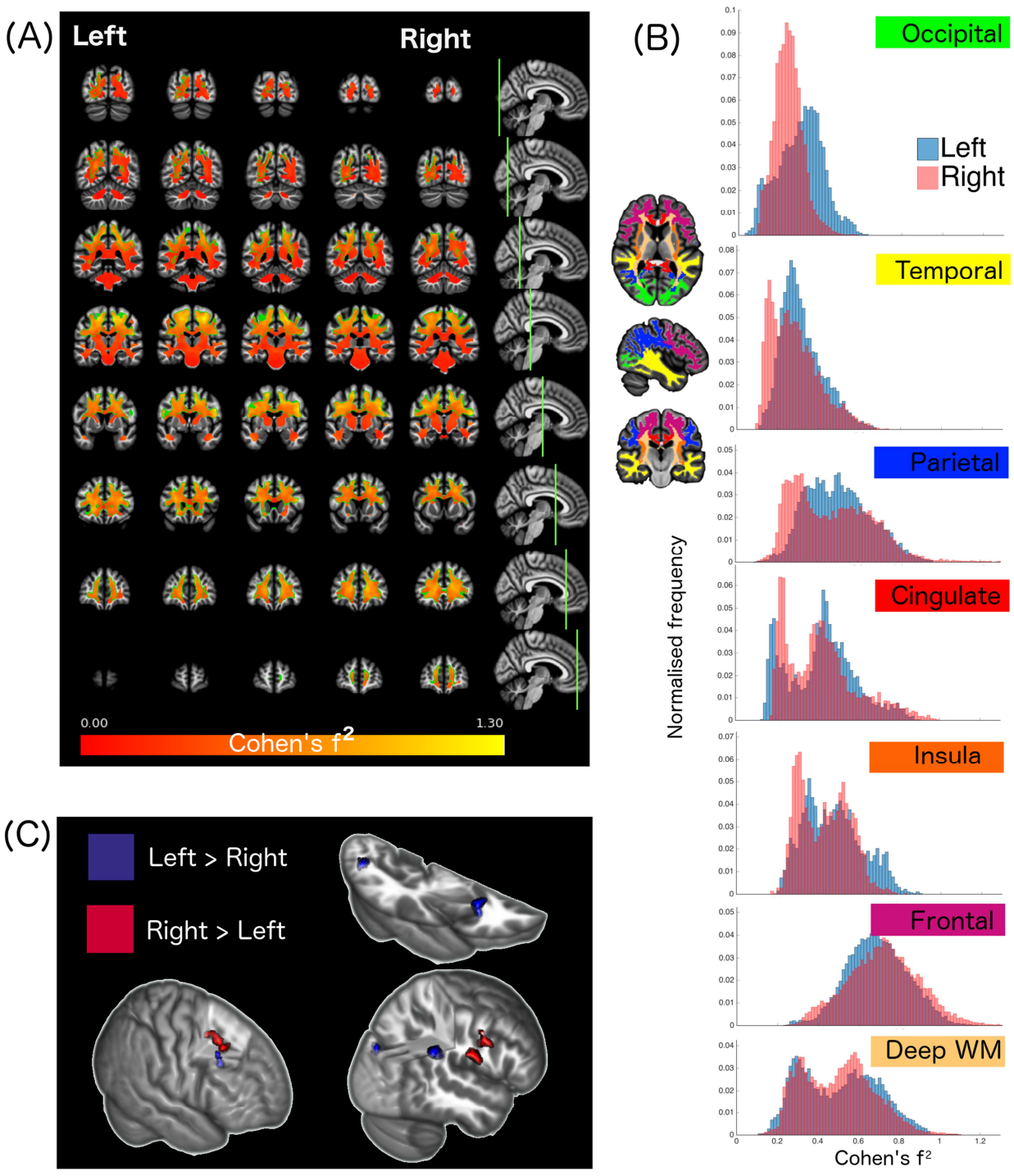

Figure 3. **Age-related effect size** (A) Spatial map of effect sizes. Location of the coronal slices shown on the right refers to the (adjacent) rightmost column of the spatial maps. The green edge encircles the areas where the effect of ageing was significant (as shown in Figure 2). (B) Distribution of effect sizes in white matter parcels. (C) Locations of significant differences in effect size between left and right hemispheres. The title of each histogram is colour-coded relative to the white matter parcel, as shown in the brain's map.

3.3 Spatio-temporal characteristics of the age-related differences

The results of polynomial fitting suggest distinct spatio-temporal patterns of age-related differences in lateral and ventral white matter. The analyses using segmented linear fitting demonstrate this point in greater detail. The spatial maps of the segmented fit parameters in the white matter are shown in Figure 4 (also see Supplementary Figures 4-6 for high resolution maps of each parameter), and examples of these fits superimposed over polynomial fits in Figure 5A (i)-(iii). The distribution of segmented fit breakpoints, which is bimodal in its form (Figure 5B – (i)), reveals a lateral-to-ventral gradient, such that earlier breakpoints, occurring at around 45 years of age, are found in lateral areas of white matter whereas later breakpoints, occurring at around 58 years of age, are found in ventral areas. The earliest breakpoints (around 37 years of age) could be observed in the left occipital and bilateral orbitofrontal white matter regions, overlapping with posterior and anterior segments of inferior fronto-occipital fasciculus, respectively. Breakpoint values were associated with the rate of change of age-related MT differences before and after the breakpoint (Figure 5B (ii)-(iii)). More lateral regions, especially the frontal areas, showed a continued MT increase before an early breakpoint (rate of change before breakpoint > 0), followed by a decrease at a relatively slow rate. Conversely, deeper and more ventral white matter areas showed no MT increase (rate of change before breakpoint ≈ 0) up to a later stage, followed by a decrease at a rapid rate. In all trajectories, the rate of change after the breakpoint was always negative, indicating that no region showed an MT increase following the trajectory bending. There was a positive association between the breakpoint and the strength of the mean (across-participants) MT intensity ($r = .54$), indicating that later breakpoints occurred in regions with more MT concentration.

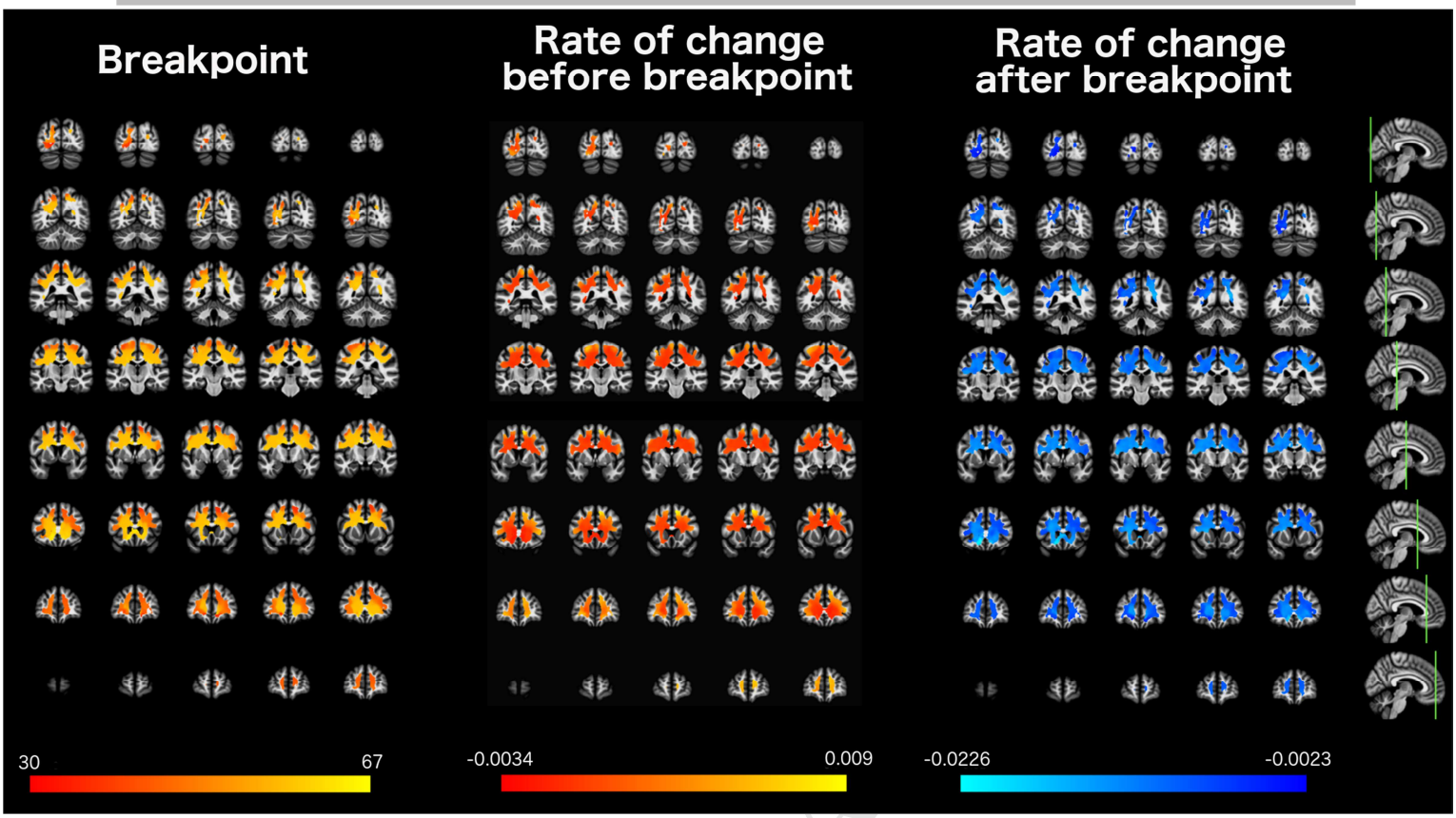

Figure 4. Spatial maps of the parameters of the segmented fit. Location of the coronal slices shown on the right refers to the rightmost columns of the spatial maps (for higher resolution images - see Supplementary Figures S4-S6).

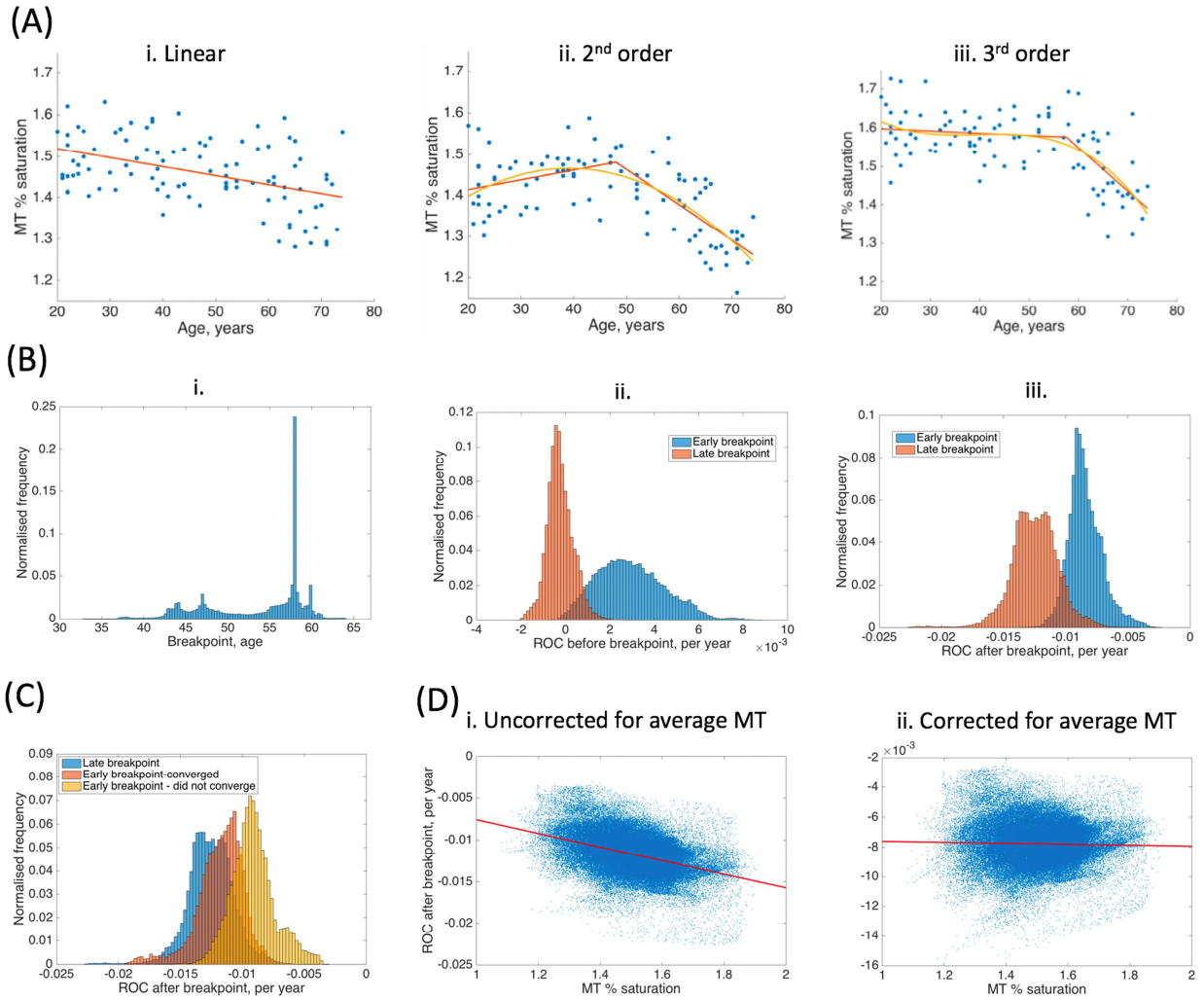

Figure 5. (A) Examples of fits from representative voxels. (B) A bimodal distribution of breakpoints (i) and their association with rate-of-change (ROC) before and after the breakpoint (ii - iii). (C) Distributions for three sets of voxels at the older age-range. (D) Association between average across-subject MT intensity and ROC. Dividing the rate of change by average across-sample MT consentration completely eliminates this association, suggesting a strictly proportional relationship between the two.

Given that a linear approximation to the trajectory after breakpoint may conceal its curvilinearity, we also considered a more refined approximation for those brain areas which demonstrated an early (less than 52 years) breakpoint. The analysis aimed to determine whether there was an actual difference at an older age range between the rate of change of the trajectory describing age-related differences in the more lateral voxels showing an early breakpoint and the rate of change in regions associated with a later breakpoint. For this purpose, we refitted the segmented fit to these voxels, considering only participants whose age was greater than the

estimated breakpoint. The segmented fit converged to the values which were not at the extremes of the fitted age-range in 41% of voxels. For the voxels that did not converge, we fitted a simple linear regression based only on participants who were 52 years-old and above (38 participants). As Figure 5C suggests, the voxels where the segmented fit converged show a rate of change more similar to voxels with a late breakpoint. This was not the case for the voxels without convergence. Across all white matter voxels the rate of change at an older age-range was negatively associated with the average across-subjects MT intensity, r = - 0.42 (Figure 5D - (i)). Importantly, their association was strictly proportional: after dividing the rate of change by the average across-sample MT intensity, this association completely disappears, r = - 0.03 (Figure 5D - (ii)).

3.4 Comparison of a one-breakpoint model fit to a two-breakpoint fit

Lastly, we considered whether one-breakpoint (two-component) segmented fit may not have been sufficient to model critical points on the trajectory describing age-related differences. We compared one-breakpoint model's goodness-of-fit to a two-breakpoint (three-segment) model's using Akaike Information Criterion. The analysis revealed two areas where a two-breakpoint model outperformed the one-breakpoint model (Figure 6-A): one was located in the deep white matter of superior corona radiata, overlapping considerably with the path of the corticospinal tract; the other, of a considerably smaller extent, was observed in the orbitofrontal white matter, in the proximity of regions showing the earliest breakpoint for the one-breakpoint model, but not overlapping with them. Both patterns were left-hemisphere dominant but differed in their temporal features (Figure 6-B). For the deep white matter region, MT decreased until the age of 32.6 on average, followed by an increase until the age of 57.7 on average, and then followed by a decrease. In the orbitofrontal area, MT increased before the first breakpoint (at the mean age

of 28.1 years) followed by a shallow decrease till the second breakpoint (at the mean age of 60.2 years), and then followed by a decrease.

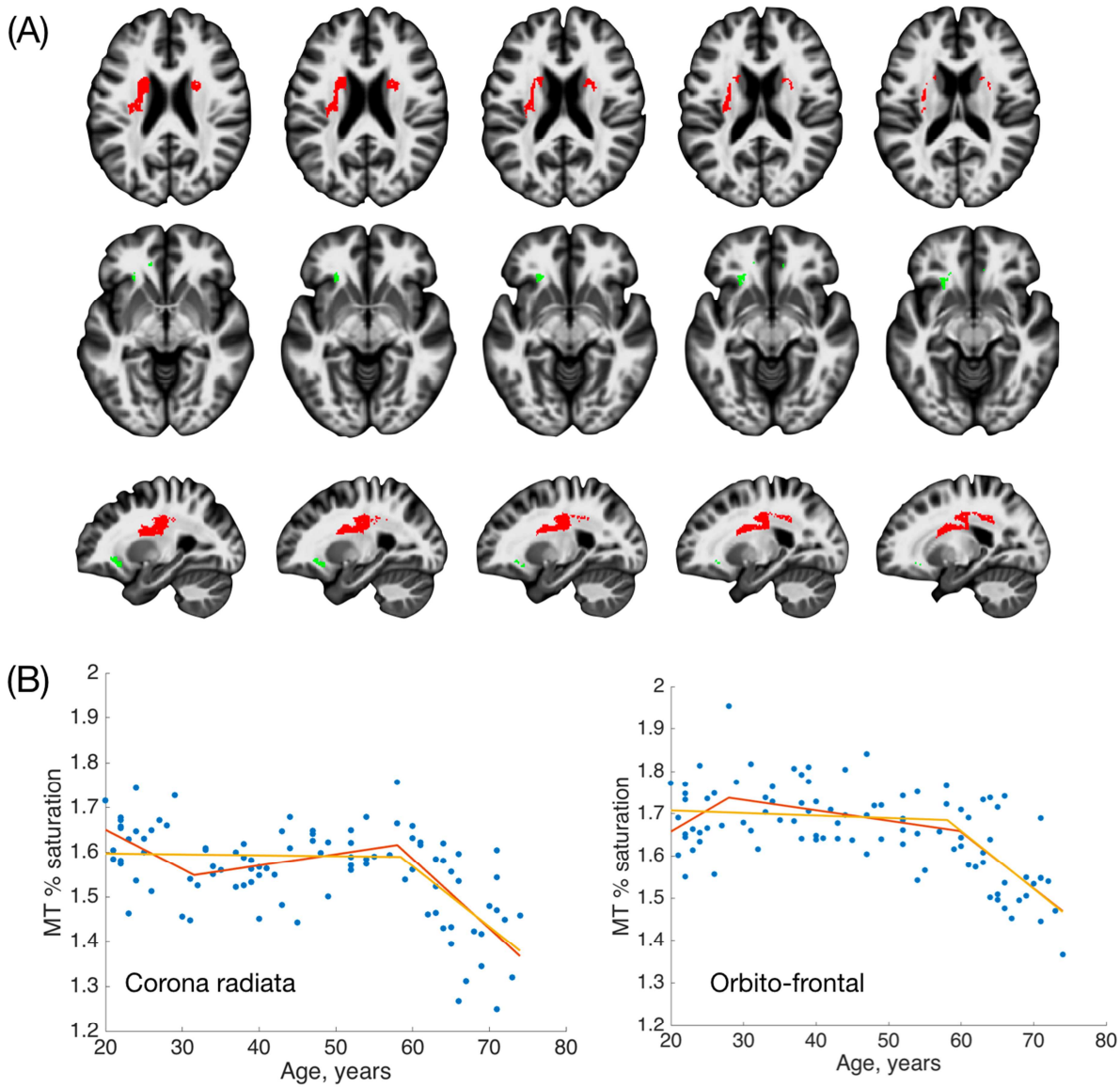

Figure 6. (A) Two-breakpoint model maps. Left is left (B). Examples of one- and two-breakpoint fits from representative voxels in corona radiata and orbito-frontal white matter.

4. DISCUSSION

In the present study, we investigated the temporal and spatial features that characterise age-related differences in myelin-sensitive MT maps in a cross-sectional cohort of adults ranging from 20 to 74 years old. Widespread age-dependent alterations in such maps have previously been reported (Callaghan et al, 2014), but their spatiotemporal properties have not yet been characterised. Using evidence from developmental studies (Deoni et al, 2011; Kinney et al, 1988; Kostovic and Jovanov-Milošević 2006; Yakovlev and Leours 1967) and on the basis of the 'last in, first out' principle, we predicted that a detailed analyses of the trajectories describing age-relative differences in the myelin sensitive maps may reveal lateral-to-ventral and left-to-right spatial gradients of healthy ageing, in addition to an anterior-to-posterior gradient.

As predicted, we found widespread age-related MT decrease in the frontal lobe. Given that changes in MT contrast are associated with increases/decreases in myelin content (Ou et al., 2009; Schmierer et al., 2007; 2008), these findings suggest a particular sensitivity of frontal myelin to the effect of ageing as compared, for instance, to occipital myelin. Furthermore, white matter parcels, which extend in the anterior-posterior direction, namely the deep white matter and regions under the insular and cingulate cortices, revealed bimodal distributions of effect size with more age-affected regions situated frontally. The main deviation from this pattern was the parietal MT where a considerable number of voxels showed a significant age-related effect. This is however not surprising given that frontal and parietal regions are organised into functional systems involved in higher cognitive abilities, such as working memory (Owen et al., 2005); according to the Flechsig's Law, (Flechsig, 1901), the developmental changes of functionally coupled anatomical regions proceeds in parallel. Interestingly, our results showed a rather moderate ageing effect in the temporal lobe, consistent with some previous reports (Sexton et al, 2014), and suggesting that brain regions showing myelin loss in healthy aging are

topographically different from the areas where neurodegeneration occurs (e.g., Huang et al, 2007; Sturm et al, 2013; Wisse et al, 2014).

There was no sufficient evidence for a left-to-right gradient of ageing in white matter myelin. Previous studies suggested that language networks, with their (typically) left hemisphere lateralisation, develop for longer (Gogtay et al, 2004; Sowell et al., 2003). In line with these results, a hemispheric asymmetry has also been shown in postnatal changes in parietal, temporal and occipital myelin-sensitive maps (Deoni et al, 2011), suggesting that age-related differences myelin may be more pronounced in the left hemisphere. We found a wider spread of statistically significant differences in the posterior left hemisphere. However, a direct comparison with the right hemisphere showed only local differences in the strength of age-related effects. These differences are difficult to interpret due to known limitations in the voxelwise precision of white matter regional alignment. Future research could benefit from integrating imaging modalities assessing myelination with diffusion-weighted imaging in order to provide a more accurate anatomical delineation of white matter structures.

Finally, the analysis of the temporal properties of the trajectories describing age-related differences revealed a lateral-to-ventral gradient . The age-related decrease in MT occurred earlier in lateral areas of white matter, likely to be dominated by cortico-cortical connection, relative to ventral areas, which are dominated by thalamo-cortical connections and fibres of corona radiata. In support of this, there was a positive association between the breakpoint and the strength of the mean (across-participants) of MT intensity, suggesting that the myelin-rich areas are more likely to have a late breakpoint. The lateral white matter regions followed a ‘growth – peak – decline’ trajectory, with a peak occurring at around 45.5 years old, followed by a relatively slow rate of age-related differences. In contrast, ventral white matter areas showed relatively stable MT levels till a later stage (around late 50s), suggesting that these areas

matured earlier than the age range we studied. The late breakpoint in these areas was followed by a rapid rate of change in age-related differences.

We also note that our results challenge the proposal that late maturing regions decline at an accelerated rate (e.g. Bender, Völkle, & Raz, 2016; Douaud et al, 2014) when this refers to age-related differences identified by myelin-sensitive white matter maps. Areas with an early breakpoint showed a moderate rate of MT decrease compared to areas with a later breakpoint. A more detailed analysis focusing on the later age range demonstrated that these rates were strictly proportional to the average voxelwise MT concentration; that is, at a later age the rate of MT decrease was equal across regions showing significant age-related differences once the voxelwise concentration was taken into account. This suggests that the defining factor is the presence of a proportional relationship between MT concentration and its age-dependent decrease rather than a greater vulnerability of the ventral regions to ageing at a late age range. It is however possible that no evidence of an accelerated decline is due to sample differences. In the present study, participants had no known health issues and the upper age limit was younger than in other studies (e.g., Douaud et al, 2014), thereby reducing the likelihood of having participants with subclinical manifestations of age-related pathologies which may be related to an accelerated rate of age-related brain changes.

The results of the present study may help delineating temporal boundaries between the duration of maturation and the onset of ageing. Animal studies showed that the adult-born oligodendrocytes continue to synthesise myelin, indicating that myelin genesis persists during adult life (Rivers et al, 2008). The exact time when maturation ends in the human brain is not defined, though previous studies suggest that it continues at least up to the beginning of the fourth decade of life (Somel et al. 2009; Lebel and Beaulieu, 2011). Protracted development of brain networks involved in high-order cognition may underpin the emergence of human-specific

cognitive abilities (Langer, 2006; Montagu, 1955). Our data suggest that the maturation range may extend to the mid-forties, since MT increase in the lateral white matter indicates myelin growth up to the age of 45, subject to limitations of the cross-sectional design. An MT decrease which follows this estimated end of maturation is also consistent with other findings from animal studies (Peters et al, 2001), showing that lately formed myelin is not stable. As for the onset of cognitive ageing, the study by Singh-Maoux et al (2012) suggests that age-related cognitive decline in high level cognitive function is detectable from the late forties, whereas other research suggests that impoverished cognitive performance as a result of healthy aging does not occur before the age of 60 (Hedden and Gabrieli, 2004). Both estimates are consistent with our finding of two age-related patterns in the myelin-sensitive maps, i.e., a moderate decrease in lateral areas starting in the mid-forties and the onset of a rapid age-related MT decrease in ventral areas in the late fifties.

We also found a few notable deviations from the generic patterns of ageing described above. Firstly, a proportion of voxels showing significant age-related effects were best fitted by the linear model. Secondly, two - predominantly left-lateralised - areas were better fitted with a two-breakpoint (three-segment) model than a one-breakpoint model. One was situated in the orbitofrontal white matter and the other in a segment of the corona radiata, considerably overlapping with the cortico-spinal tract. These findings warrant further investigation as the age-range explored in the present study may have also affected the results, especially in brain areas showing linear patterns of age-related differences. Non-linear trajectories may have been difficult to identify here simply because none of our participants was old enough to reveal them; a visual inspection of the data shown in Figure 5A (i) offers some support for this interpretation. The investigation of the extent and configurations of the two-breakpoint patterns would also benefit from an extended age-range. However, it is important to note that the finding of patterns which contain an additional early breakpoint are in line with previous studies showing the onset

of age-related decrements in some cognitive domains (e.g., perceptual and motor speed) from as early as the 2nd decade of life (Salthouse, 2000).

The cross-sectional design is limited in the conclusions it can draw due to between-subject variability being confounded with ageing effects. Longitudinal studies are needed to validate and refine the results reported here (Bender, Völkle, & Raz, 2016). Moreover, we note that the investigation of myelin changes cannot be complete at the mesoscale afforded by the resolution of myelin-sensitive maps and should be complemented with histological studies of the underlying microscale processes (i.e., ballooning, splitting of the myelin sheath).

In conclusion, our novel analyses of MT maps identified and quantified the spatial and temporal features characterising structural changes in the ageing brain at a microstructural level. In addition to the anterior-to-posterior gradient of white matter age-related differences, a lateral-to-ventral gradient was also observed, in line with the temporal sequence of connectivity development and myelogenesis. The temporal characteristics of a lateral-to-ventral gradient did not fit the proposal that areas which mature later decline at an accelerated rate. Instead, brain areas which mature early and show small age-related changes over most of the adult life-span demonstrated a rapid MT decrease at a later age.

ACKNOWLEDGMENTS

This work was supported by a Royal Society Dorothy Hodgkin Fellowship (502008.K518/SLB) and Research Grant (MC), the Wellcome Trust (GR); the European Research Council under the European Union's Seventh Framework Programme (FP7/2007-2013) / ERC grant agreement n° 616905 (NW); the WT PRF 097720/Z/11/Z, MRC project grant MR/M023672/1, and the Stroke Association project grant TSA 2014/02 (TH); The Wellcome Trust Centre for Neuroimaging is supported by core funding from the Wellcome Trust 091593/Z/10/Z.

The authors declare no conflict of interest.

REFERENCES

Avants BB, Tustison NJ, Song G, Cook PA, Klein A, Gee JC. A reproducible evaluation of ANTs similarity metric performance in brain image registration. NeuroImage 2011;54:2033-2044.

Bender AR, Völkle MC, Raz N. Differential aging of cerebral white matter in middle-aged and older adults: A seven-year follow-up. NeuroImage 2016;125:74-83

Basser PJ, Mattiello J, LeBihan D. MR diffusion tensor spectroscopy and imaging. Biophys J 1994;66:259–267.

Bigler ED, Blatter DD, Anderson CV, Johnson SC, Gale SD, Hopkins RO, Burnett B. Hippocampal Volume in Normal Aging and Traumatic Brain Injury. American Journal of Neuroradiology 1997;18:11-23.

Brickman AM, Meier IB, Korgaonkar MS, Provenzano FA, Grieve SM, Siedlecki KL, Wasserman BT, Williams LM, Zimmerman ME. Testing the white matter retrogenesis hypothesis of cognitive aging. Neurobiol Aging 2012;33:1699-715.

Callaghan M, Freund P, Draganski B, Anderson E, Cappelletti M, Chowdhury R, Diedrichsen J, Fitzgerald T, Smittenaar P, Helms G, Lutti A, Weiskopf N. Wide-spread age-related changes of the microstructure in the human brain revealed by quantitative MRI. Neurobiology of Ageing 2014a;35:1862-72.

Casey BJ, Giedd JN, Thomas K. Structural and functional brain development and its relation to cognitive development. Biological Psychology 2000;54:241-257.

Catani M, Dell'Acqua F, Vergani F, Malik F, Hodge H, Roy P, Valabregue R, Thiebaut de Schotten M. Short frontal lobe connections of the human brain. Cortex 2012;48:273-91.

Davis SW, Dennis NA, Daselaar SM, Fleck MS, Cabeza R. Qué PASA? The posterior–anterior shift in aging. Cerebral Cortex 2008;18:1201–1209.

Deoni SC, Rutt BK, Arun T, Pierpaoli C, Jones DK. Gleaning multi-component T1 and T2 information from steady-state imaging data. Magnetic Resonance Medicine 2008;60:1372–1387.

Deoni S, Mercure E, Blasi A, Gasston D, Thomson A, Johnson M, Williams S, Murphy D. Mapping Infant Brain Myelination with Magnetic Resonance Imaging. Journal of Neuroscience 2011;31:784-791.

Douaud G, Jbabdi S, Behrens TEJ, Menke RA, Gass A, Monsch A, Whitcher B, Kindlmann G, Matthews PM, Smith S. DTI measures in crossing-fibre areas: *Increased* diffusion anisotropy reveals early white matter alteration in MCI and mild Alzheimer's disease. NeuroImage 2011;55:880-890.

Douaud G, Groves AR, Tamnes CK, Westlye LT, Duff EP, Engvig A, Walhovd KB, James A, Gass A, Monschg AU, Matthews PM, Fjell AM, Smith SM, Johansen-Berg H. A common brain network links development, aging, and vulnerability to disease. PNAS 2014;11:17648-17653.

Draganski B, Ashburner J, Hutton C, Kherif F, Frackowiak RSJ, Helms G, Weiskopf N. Regional specificity of MRI contrast parameter changes in normal ageing revealed by voxel-based quantification (VBQ). Neuroimage 2011;55:1423–34.

Eklund A, Andersson M, Josephson C, Johannesson M, Knutsson H. Does parametric fMRI analysis with SPM yield valid results? - An empirical study of 1484 rest datasets. NeuroImage 2012;61:565-578.

Fjell AM, McEvoy L, Holland D, Dale AM, Walhovd KB; Alzheimer's Disease Neuroimaging Initiative. What is normal in normal aging? Effects of aging, amyloid and Alzheimer's disease on the cerebral cortex and the hippocampus. Prog Neurobiol 2014;117:20-40.

Flechsig P, Developmental (myelogenetic) localisation of the cerebral cortex in the human subject. Lancet 1901; 158: 1027-1030.

Folstein MF, Folstein SE, McHugh PR. 'Mini-mental state'. A practical method for grading the cognitive state of patients for the clinician. Journal of Psychiatric Res 1975;12:189-98.

Gogtay N, Giedd N, Lusk L, Hayashi K, Greenstein D, Vaituzis A, Nugent TFIII, Herman DH, Clasen LS, Toga AW, Rapoport JL, Thompson PM. Dynamic mapping of human cortical development during childhood through early adulthood. PNAS 2004;101:8174-8179.

Head D, Buckner RL, Shimony JS, Williams LE, Akbudak E, Conturo TE, McAvoy M, Morris JC, Snyder AZ. Differential Vulnerability of Anterior White Matter in Nondemented Aging with Minimal Acceleration in Dementia of the Alzheimer Type: Evidence from Diffusion Tensor Imaging. Cerebral Cortex 2004;14:410–423.

Hedden T, Gabrieli JDE. Insights into the ageing mind: a view from cognitive neuroscience. Nat Rev Neurosci 2004;5:87-96.

Helms G, Dathe, H, Kallenberg K, Dechent P. High-resolution maps of magnetization transfer with inherent correction for RF inhomogeneity and T1 relaxation obtained from 3D FLASH MRI. Magn Reson Med 2008;60:1396–407.

Huang J, Friedland RP, Auchus AP. Diffusion Tensor Imaging of Normal-Appearing White Matter in Mild Cognitive Impairment and Early Alzheimer Disease: Preliminary Evidence of Axonal Degeneration in the Temporal Lobe. American Journal of Neuroradiology 2007; 28:1943-1948.

Jones DK, Knösche TK, Turner R. White matter integrity, fiber count, and other fallacies: The do's and don'ts of diffusion MRI. NeuroImage 2012;73:239–254

Keihaninejad S, Heckemann RA, Fagiolo G, Symms MR, Hajnal JV, Hammers A, and The Alzheimer's Disease Neuroimaging Initiative. A robust method to estimate the intracranial volume across MRI field strengths (1.5T and 3T). Neuroimage 2010;50:1427–1437.

Kinney HC, Brody BA, Kloman AS, Gilles FH. Sequence of central nervous system myelination in human infancy. II. Patterns of myelination in autopsied infants. J Neuropathol Exp Neurol 1988;47:217–234.

Klein A, Andersson J, Ardekani BA, Ashburner J, Avants B, Chiang MC, Christensen GE, Collins DL, Gee J, Hellier P, Song JH, Jenkinson M, Lepage C, Rueckert D, Thompson P, Vercauteren T, Woods RP, Mann JJ, Parsey RV. Evaluation of 14 nonlinear deformation algorithms applied to human brain MRI registration. Neuroimage 2009;46:786–802.

Knutsson H, Westin CF. Normalized and differential convolution: methods for interpolation and filtering of incomplete and uncertain data. Proceedings of Computer Vision and Pattern Recognition 1993, 515–523.

Kostovic I, Jovanov-Milošević N. The development of cerebral connections during the first 20–45 weeks' gestation. Semin Fetal Neonat M 2006;11:415–422.

Langer J. The heterochronic evolution of primate cognitive development. Biol Theory 2006;1:41–43.

Lebel C, Beaulieu C. Longitudinal Development of Human Brain Wiring Continues from Childhood into Adulthood. Journal of Neuroscience 2011;31:10937-10947.

Lee JE, Chung MK, Lazar M, DuBray MBA, Kim J, Bigler ED, Lainhart JE, Alexander AL. study of diffusion tensor imaging by tissue-specific, smoothing-compensated voxel-based analysis. NeuroImage 2009;44:870-883.

Lutti A, Hutton C, Finsterbusch J, Helms G, Weiskopf N. Optimization and validation of methods for mapping of the radiofrequency transmit field at 3T. Magn Reson Med 2010;64:229–38.

Lutti A, Stadler J, Josephs O, Windischberger C, Speck O, Bernarding J, Hutton C, Weiskopf N. Robust and Fast Whole Brain Mapping of the RF Transmit Field B1 at 7T. PLoS One 7 2012;e32379.

Montagu MFA. Time, morphology, and neoteny in the evolution of man. Am Anthropol 1955;57:13–27.

Ou X, Sun S-W, Liang H-F, Song S-K, Gochber DF. Quantitative magnetization transfer measured pool-size ratio reflects optic nerve myelin content in ex vivo mice. Magn Reson Med 2009; 61:364–371

Owen AM, McMillan KM, Laird AR, Bullmore E. N-back working memory paradigm: a meta-analysis of normative functional neuroimag- ing studies. Hum Brain Mapp 2005; 25:46 – 59.

Peters A, Sethares C, Killiany RJ. Effects of age on the thickness of myelin sheaths in monkey primary visual cortex. The Journal of Comparative Neurology 2001; 435:241–248.

R Core Team. R: A language and environment for statistical computing. R Foundation for Statistical Computing, Vienna, Austria. 2015;URL https://www.R-project.org

Raz N, F M Gunning D Head J H Dupuis J McQuain S D Briggs W J Loken A E Thornton J D Acker. Selective aging of the human cerebral cortex observed in vivo: differential vulnerability of the prefrontal gray matter. Cerebral Cortex 1997;7:268-82.

Raz N, Gunning-Dixon FM, Head D, Dupuis JH, Acker JD. Neuroanatomical correlates of cognitive aging: evidence from structural magnetic resonance imaging. Neuropsychology 1998;12:95-114.

Raz N. Aging of the brain and its impact on cognitive performance: Integration of structural and functional finding. In: Craik F, Salthouse T, editors. Handbook of Aging and Cognition II. Psychology Press; 2000. p. 1–90.

Raz N, Lindenberger U, Rodrigue KM, Kennedy KM, Head D, Williamson A, Dahle C, Gerstorf D, Acker JD. Regional Brain Changes in Aging Healthy Adults: General Trends, Individual Differences and Modifiers. Cerebral Cortex 2005;15:1676-89.

Reisberg B, Franssen EH, Hasan SM, Monteiro I, Boksay I, Souren LE, Kenowsky S, Auer SR, Elahi S, Kluger A. Retrogenesis: clinical, physiologic, and pathologic mechanisms in brain

aging, Alzheimer's and other dementing processes. Eur Arch Psychiatry Clin Neuroscience 1999;3:28-36.

Rivers L, Young KM, Rizzi M, Jamen F, Psachoulia K, Wade A, Kessaris N, Richardson WD. PDGFRA/NG2 glia generate myelinating oligodendrocytes and piriform projection neurons in adult mice. Nat Neu 2008;11:1392-1401.

Salat DH, Tuch DS, Greve DN, van der Kouwe AJ, Hevelone ND, Zaleta AK, Rosen BR, Fischl B, Corkin S, Rosas HD, Dale AM. Age-related alterations in white matter microstructure measured by diffusion tensor imaging. Neurobiol. Aging 2005a;26:1215–1227.

Salat DH, Tuch DS, Hevelone ND, Fischl B, Corkin S, Rosas HD, Dale AM. Age-related changes in prefrontal white matter measured by diffusion tensor imaging. Ann. N. Y. Acad. Sciences 2005b;1064:37–49.

Salthouse TA. Aging and measures of processing speed. Biol Psychol 2000; 54: 35-54

Sexton CE, Walhovd KB, Storsve AB, Tamnes CK, Westlye LT, Johansen-Berg H, Fjell AM. Accelerated changes in white matter microstructure during aging: A longitudinal diffusion tensor imaging study. J Neurosci 2014;34:15425–15436.

Shaw P, Kabani NJ, Lerch JP, Eckstrand K, Lenroot R, Gogtay N, Greenstein D, Clasen L, Evans A, Rapoport JL et al. Neurodevelopmental trajectories of the human cerebral cortex. Journal of Neuroscience 2008;28:3586–3594.

Schmierer K, Tozer DJ, Scaravilli F, Altmann DR, Barker GJ, Tofts PS, Miller DH. Quantitative magnetization transfer imaging in postmortem multiple sclerosis brain. J. Magn. Reson. Imaging 2007;26:41–51.

Schmierer K, Wheeler-Kingshott CAM, Tozer DJ, Boulby PA, Parkes HG, Yousry TA, Scaravilli F, Barker GJ, Tofts PS, Miller DH. Quantitative magnetic resonance of postmortem multiple sclerosis brain before and after fixation. Magn Reson Med 2008; 59:268–277

Schmitz TW, Spreng N and The Alzheimer's Disease Neuroimaging Initiative. Basal forebrain degeneration precedes and predicts the cortical spread of Alzheimer's pathology. Nature Communication 2016;7:13249.

Singh-Manoux A, Kivimaki M, Glymour MM, Elbaz A, Berr C, Ebmeier KP, Ferrie JE, Dugravot A. Timing of onset of cognitive decline. BMJ 2012;344,d7622.

Somel M, Franz H, Yan Z, Lorenc A, Guo S, Giger T, Kelso J, Nickel B, Dannemann M, Bahn S et al.. Transcriptional neoteny in the human brain. PNAS 2009;106:5743-5748.

Sowell ER, Peterson BS, Thompson PM, Welcome SE, Henkenius AL, Toga AW. Mapping cortical change across the human life span. Nature Neuroscience 2003;6:309–315.

Sowell ER, Thompson PM, Leonard CM, Welcome SE, Kan E, Toga AW. Longitudinal mapping of cortical thickness and brain growth in normal children. Journal of Neuroscience 2004;24:8223-31.

Sturm VE, Yokoyama JS, Seeley WW, Kramer JK, Miller BL, Rankin KP. Heightened emotional contagion in mild cognitive impairment and Alzheimer's disease is associated with temporal lobe degeneration. PNAS 2013;110:9944–9949.

Toms JD, Lesperance ML. Piecewise regression: a tool for identifying ecological thresholds. Ecology 2003;84:2034–2041

Weiskopf N, Suckling J, Williams G, Correia MM, Inkster B, Tait R, Ooi C, Bullmore ET, Lutti A. Quantitative multi-parameter mapping of R1, PD*, MT, and R2* at 3T: a multi-center validation. Frontiers in Neuroscience 2013;7:1–11.

West MJ, Coleman PD, Flood DG, Troncoso JC. Differences in the pattern of hippocampal neuronal loss in normal ageing and Alzheimer's disease. The Lancet 1994; 8925:769-772.

Wisse L, Biessels GJ, Heringa SM, Kuijf HJ, Dineke H, Koekd L, Luijtene PR, Geerlings MI, on behalf of the Utrecht Vascular Cognitive Impairment (VCI). Hippocampal subfield volumes at 7T in early Alzheimer’s disease and normal aging. Neurobiology of Aging 2014;35:2039–2045.

Yakovlev PI, Leours AR. The myelogenetic cycles of regional maturation of the brain. In: Minkowski A, editor. Regional development of the brain in early life. Oxford: Blackwell; 1967. p. 3–70.

Supplementary Figures

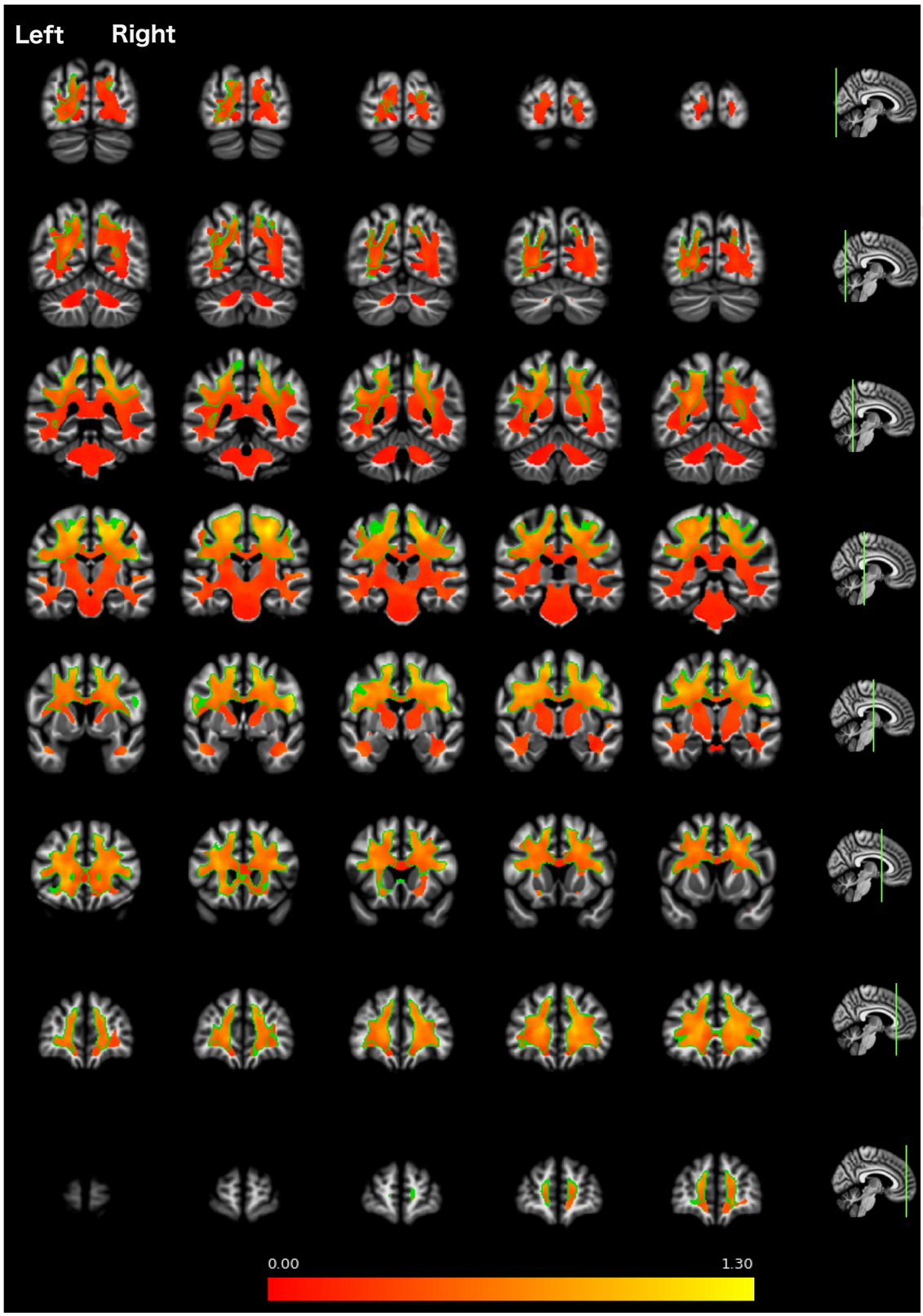

Figure S 1. **Spatial map of age-related effect size.** Location of the coronal slices shown on the right refers to the (adjacent) rightmost column of the spatial maps. The green edge encircles the areas where the effect of ageing was significant (as shown in Figure 2).

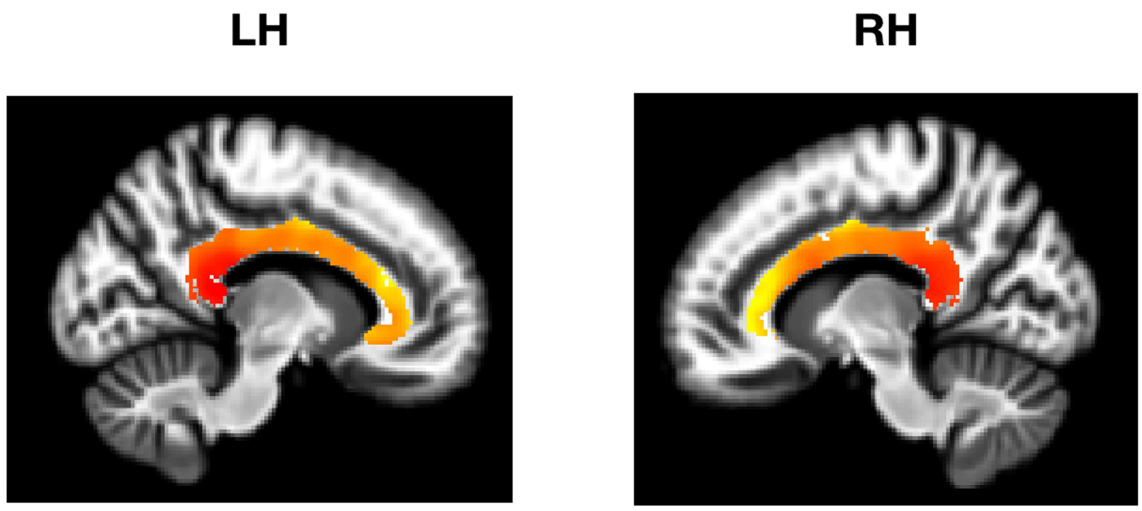

Figure S 2. Distribution of the effect sizes along the cingulate white matter. The red-to-yellow intensity is scaled between 0 and .8

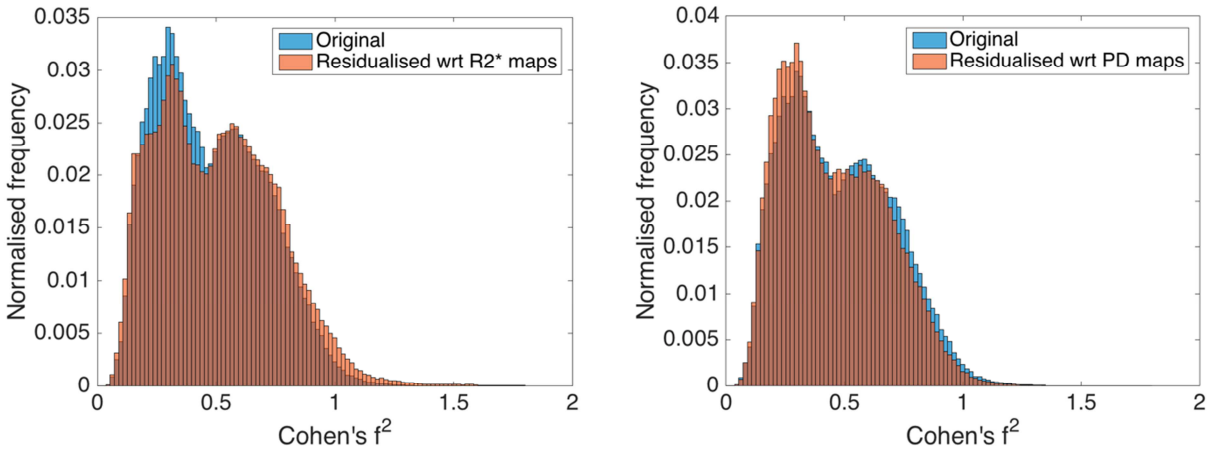

Figure S 3. Distributions of effect size before and after residualisation of MT with respect to R2* (left) and PD* (right) maps, sensitive to neurovascular and microscopic lesion alterations.

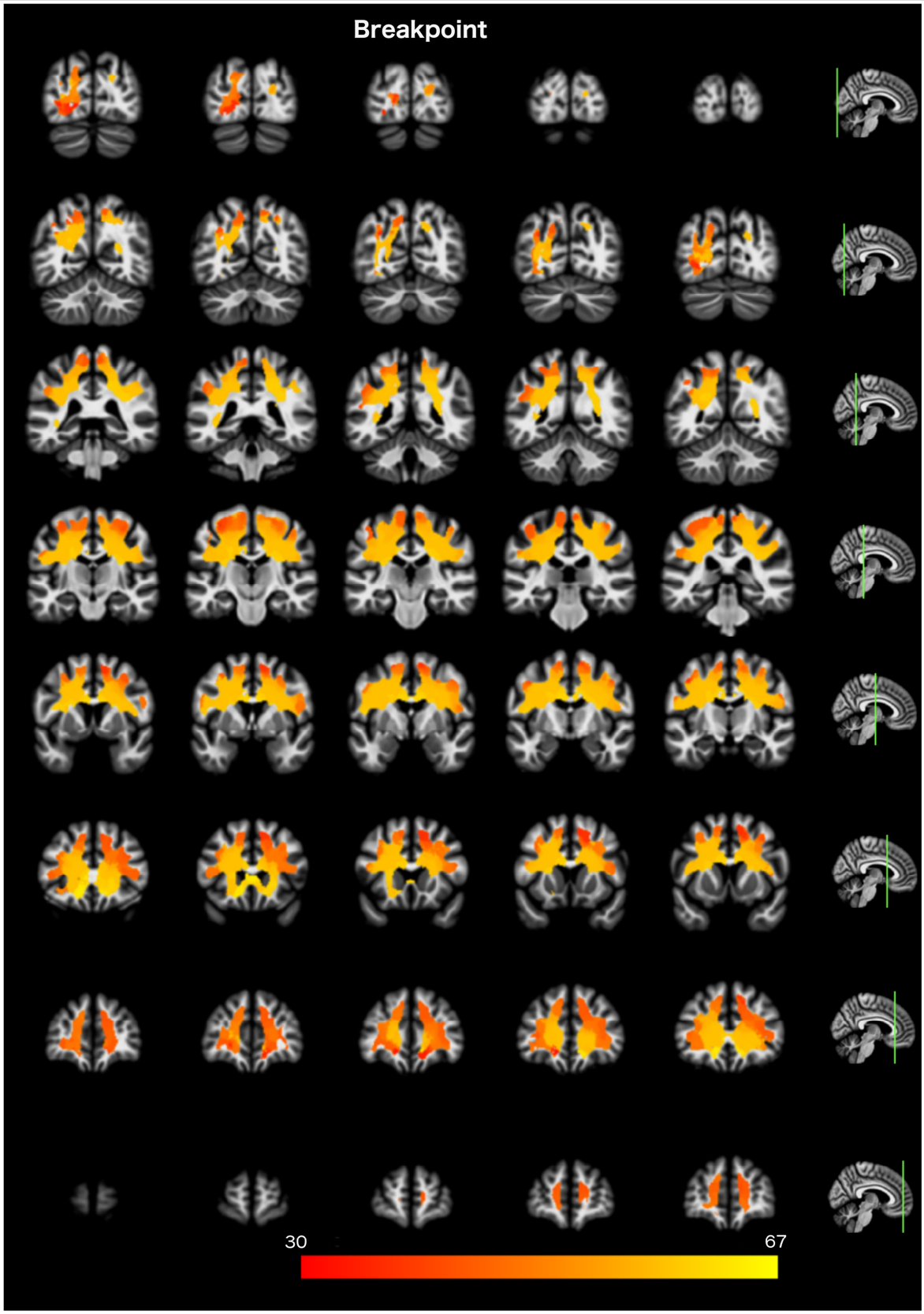

Figure S 4. **Spatial maps of the segmented fit parameter: Breakpoint**

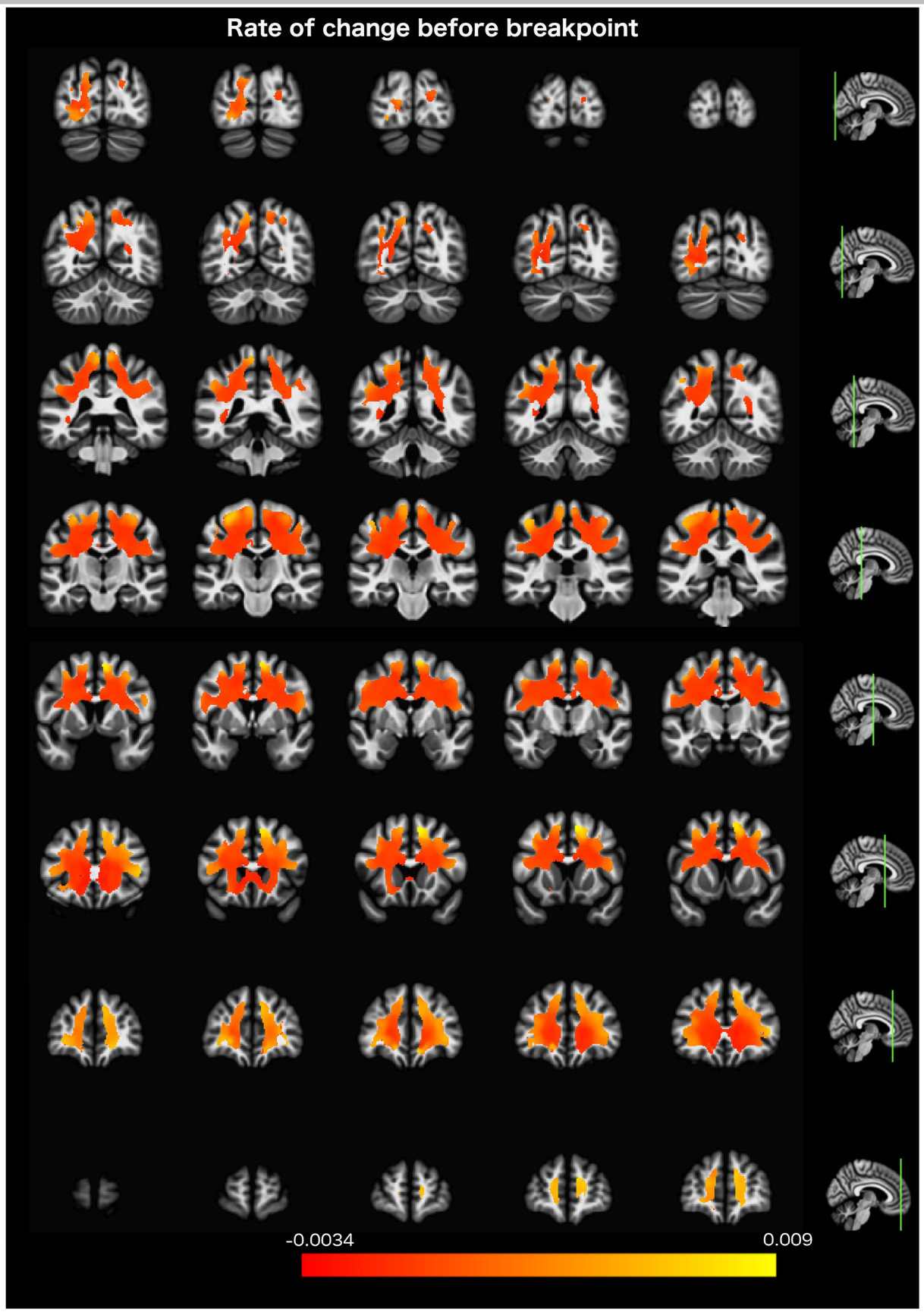

Figure S 5. **Spatial maps of the segmented fit parameter: Rate of change before breakpoint**

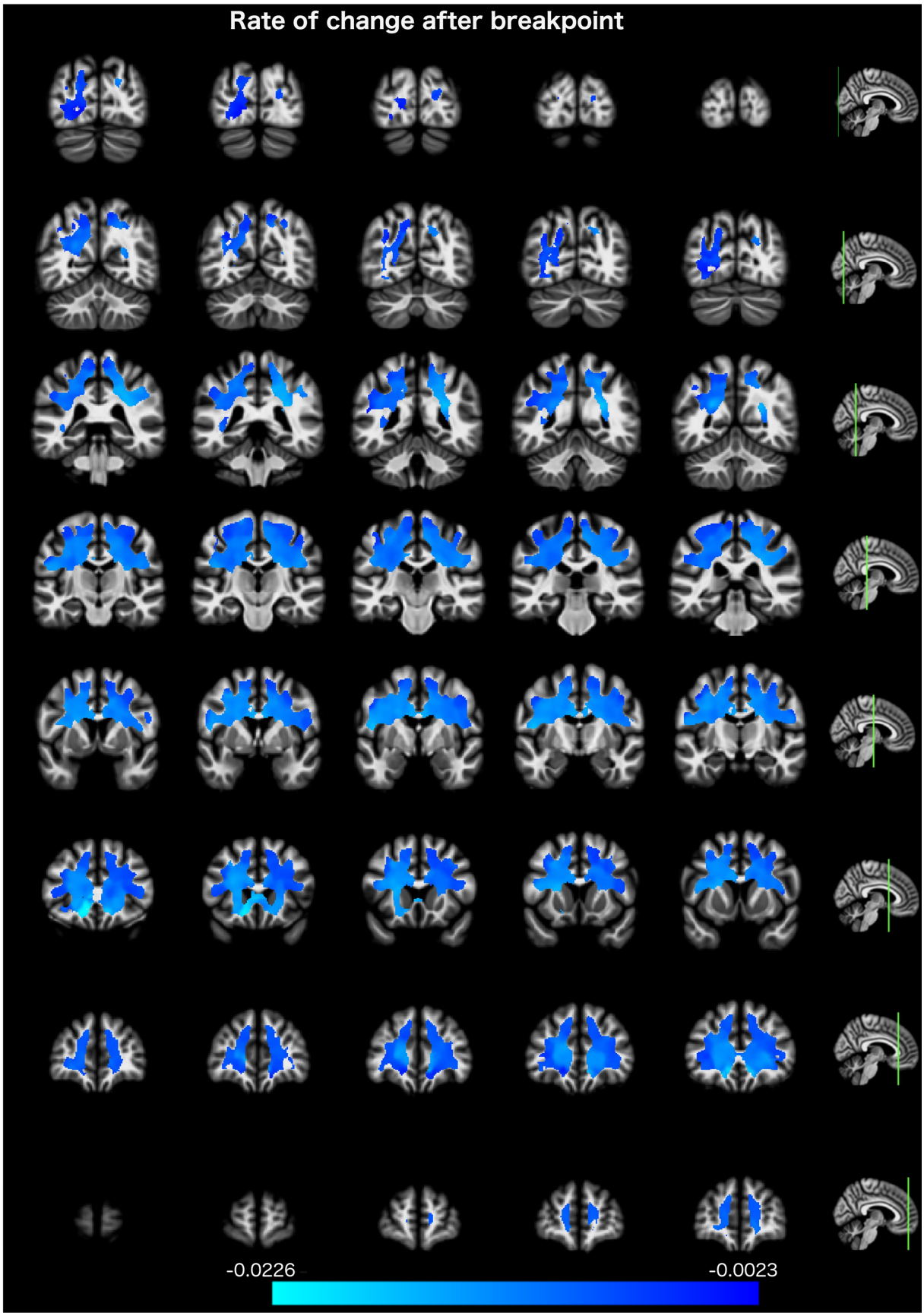

Figure S 6. **Spatial maps of the segmented fit parameter: Rate of change after breakpoint.**

SPATIAL AND TEMPORAL GRADIENTS OF HEALTHY AGEING: A STUDY OF MYELIN-SENSITIVE MAPS ACROSS THE LIFESPAN

Vyacheslav R. Karolis, Martina F. Callaghan, Jane Chieh-En Tseng, Thomas Hope, Nikolaus Weiskopf, Geraint Rees, Marinella Cappelletti

HIGHLIGHTS

- We studied spatial gradients of white matter ageing in myelin-sensitive MT maps
- We found evidence for two gradients: anterior-to-posterior and lateral-to-ventral
- In the lateral white matter maturation continues up to the age of 45
- These late-maturing white matter regions show an early but gradual MT decrease
- Instead, early-maturing ventral regions show a rapid MT decrease at a later age